

Investigating the Molecular Mechanisms of In-Plane Mechanochemistry on Cantilever Arrays

Moyu Watari,[†] Jane Galbraith,[‡] Hans-Peter Lang,^{§,||} Marilyne Sousa,^{||} Martin Hegner,[§] Christoph Gerber,[§] Mike A. Horton,[†] and Rachel A. McKendry^{*,†}

Contribution from the London Centre for Nanotechnology and Department of Medicine, University College London, 5 University Street, London WC1E 6JJ, U.K., Department of Statistical Science, University College London, Gower Street, London WC1E 6BT, U.K., National Center of Competence in Research (NCCR) on Nanoscale Science, Institute of Physics, University of Basel, Klingelbergstrasse 82, CH-4056 Basel, Switzerland, and IBM Research GmbH, Zurich Research Laboratory, Säumerstrasse 4, CH-8803 Rüschlikon, Switzerland

Received July 20, 2006; E-mail: r.a.mckendry@ucl.ac.uk

Abstract: Free-standing cantilevers, which directly translate specific biochemical reactions into micromechanical motion, have recently attracted much attention as label-free biosensors and micro/nano robotic devices. To exploit this mechanochemical sensing technology, it is essential to develop a fundamental understanding of the origins of surface stress. Here we report a detailed study into the molecular basis of stress generation in aqueous environments focusing on the pH titration of model mercaptohexadecanoic acid self-assembled monolayers (SAMs), using *in situ* reference cantilevers coated with nonionizable hexadecanethiol SAMs. Semiautomated data analysis and a statistical model were developed to quantify cyclic deprotonation/protonation reactions on multiple arrays. In-plane force titrations were found to have the sensitivity to detect ionic hydrogen bond formation between protonated and nonprotonated carboxylic acid groups in the proximity of the surface $pK_{1/2}$, which generated a mean tensile differential surface stress of $+1.2 \pm 0.3$ mN/m at pH 6.0, corresponding to 1 pN attractive force between two adjacent MHA molecules. Conversely, the magnitude of compressive differential surface stress was found to increase progressively with pH ≥ 7.0 , reaching a maximum of -14.5 ± 0.5 mN/m at pH 9.0, attributed to enhanced electrostatic repulsion between deprotonated carboxylic acid groups. However, striking differences were observed in the micromechanical responses to different ionic strength and ion species present in the aqueous environment, highlighting the critical role of counter- and co-ions on surface stress. Our findings provide fundamental insights into the molecular mechanisms of in-plane mechanochemistry, which may be exploited for biosensing and nanoactuation applications.

Introduction

When a chemical or biological reaction occurs on one surface of a cantilever, a surface stress is generated, which causes the deflection of the free-end of the beam. The range of biological systems, which have been probed via this novel sensing mechanism, extends from DNA hybridization^{1–5} to protein recognition^{1,6–8} and cell adhesion,^{9,10} but there is much debate in the literature about the underlying molecular transduction mechanisms. To realize potential sensor and microrobotic

applications, it is essential to learn to control both the direction and amplitude of cantilever motion. It has been proposed that electrostatic interactions play an important role in surface stress,^{1,2,5} yet interpretation of measurements is hindered by the inherent complexity of biomolecules with multiple functional and zwitterionic groups. In contrast, alkanethiols form well-defined SAMs on gold surfaces, where the surface properties are controlled by the chain length and terminal group.^{11,12,15} In

[†] London Centre for Nanotechnology and Department of Medicine, University College London.

[‡] Department of Statistical Science, University College London.

[§] University of Basel.

^{||} Zurich Research Laboratory.

- (1) Fritz, J.; Baller, M. K.; Lang, H.-P.; Rothuizen, H.; Vettiger, P.; Meyer, E.; Güntherodt, H.-J.; Gerber, C.; Gimzewski, J. K. *Science* **2000**, *288*, 316–318.
- (2) McKendry, R. A.; Zhang, J.; Arntz, Y.; Strunz, T.; Hegner, M.; Lang, H.-P.; Baller, M. K.; Certa, U.; Meyer, E.; Güntherodt, H.-J.; Gerber, C. *Proc. Natl. Acad. Sci. U.S.A.* **2002**, *99*, 9783–9788.
- (3) Fritz, J.; Cooper, E. B.; Gaudet, S.; Sorger, P. K.; Manalis, S. R. *Proc. Natl. Acad. Sci. U.S.A.* **2002**, *99*, 14142–14146.
- (4) Mukhopadhyay, R.; Lorentzen, M.; Kjems, J.; Besenbacher, F. *Langmuir* **2005**, *21*, 8400–8408.

- (5) Shu, W.; Liu, D.; Watari, M.; Riener, C. K.; Strunz, T.; Welland, M. E.; Balasubramanian, S.; McKendry, R. A. *J. Am. Chem. Soc.* **2005**, *127*, 17054–17060.
- (6) Backmann, N.; Zahnd, C.; Huber, F.; Bietsch, A.; Plüchthun, A.; Lang, H.-P.; Güntherodt, H.-J.; Hegner, M.; Gerber, C. *Proc. Natl. Acad. Sci. U.S.A.* **2005**, *102*, 14587–14592.
- (7) Wu, G. H.; Ji, H. F.; Hansen, K.; Thundat, T.; Datar, R.; Cote, R.; Hagan, M. F.; Chakraborty, A. K.; Majumdar, A. *Proc. Natl. Acad. Sci. U.S.A.* **2001**, *98*, 1560–1564.
- (8) Savran, C. A.; Knudsen, S. M.; Ellington, A. D.; Manalis, S. R. *Anal. Chem.* **2004**, *76*, 3194–3198.
- (9) Ilic, B.; Yang, Y.; Craighead, H. G. *Appl. Phys. Lett.* **2004**, *85*, 2604–2606.
- (10) Park, J.; Ryu, J.; Choi, S. K.; Seo, E.; Cha, J. M.; Ryu, S.; Kim, J.; Kim, B.; Lee, S. H. *Anal. Chem.* **2005**, *77*, 6571–6580.
- (11) Nuzzo, R. G.; Allara, D. L. *J. Am. Chem. Soc.* **1983**, *105*, 4481–4483.
- (12) Bain, C. D.; Troughton, E. B.; Tao, Y.-T.; Evall, J.; Whitesides, G. M.; Nuzzo, R. G. *J. Am. Chem. Soc.* **1989**, *111*, 321–335.

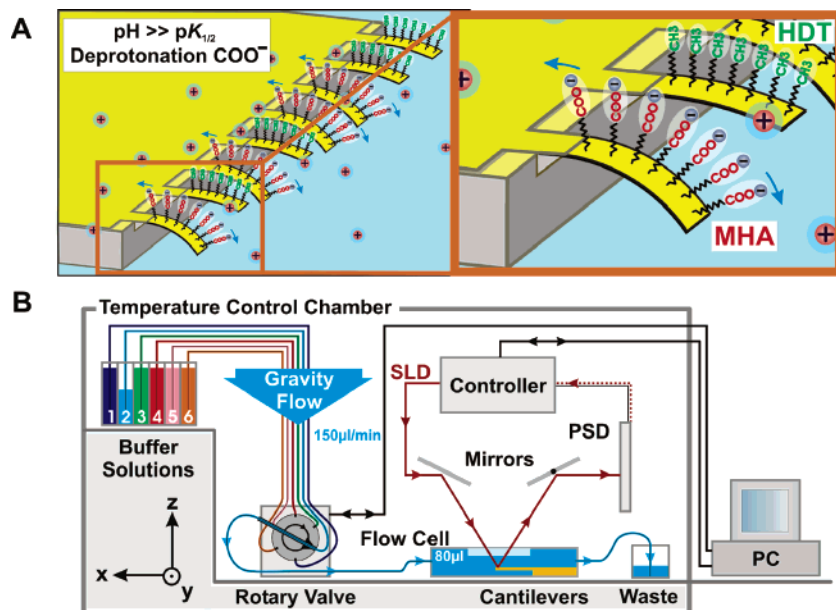


Figure 1. (A) Schematic figure to illustrate the principle of differential surface stress titration of MHA, using reference HDT coated cantilevers. (B) Experimental apparatus to optically detect cantilever bending in different liquid environments.

particular, the acid–base properties of carboxylic acid terminating SAMs such as mercaptohexadecanoic acid, which can be controlled via the pH of the liquid environment, offer an ideal system for fundamental studies with broad applicability to colloidal science, catalysis, protein folding, and membrane biophysics. Although acid–base reactions of SAMs have previously been studied on cantilevers, results have varied widely^{13,14} and have been typically limited due to either lack of mechanical sensitivity or the use of only single cantilever measurements. Single cantilever measurements are notoriously problematic because nonspecific reactions, including changes in temperature, refractive index, and reactions occurring on the underside of a cantilever can dominate the value of an absolute signal. Differential measurements using *in situ* reference cantilevers have been shown to be essential to detect chemically specific surface forces and enable multiple reactions to be probed in parallel, under similar experimental conditions.^{1,2,5,6,14} Fritz et al. reported differential investigations of surface stress on SAMs, but only repulsive forces were detected in one aqueous environment and no statistical analysis was performed.¹⁴ Many fundamental questions remain concerning the mechanisms of pH-triggered in-plane bonding and surface stress action along the cantilever. How strong are the in-plane forces associated with the surface $pK_{1/2}$, at which half the population of terminal carboxylic acid groups will be protonated and half are deprotonated? Further, how are these forces influenced by the presence of anions and cations in the aqueous solution?

Multiple arrays of eight rectangular silicon (100) cantilevers, each measuring 500 μm in length, 100 μm in width, and 0.9 μm in thickness with a nominal spring constant of 0.02 N/m, were coated on one side with a thin film of gold (20 nm gold with a 2 nm titanium adhesion layer). Individual cantilevers were functionalized with either mercaptohexadecanoic acid (HS-

$(\text{CH}_2)_{15}\text{COOH}$, herein termed MHA) or hexadecanethiol (HS- $(\text{CH}_2)_{15}\text{CH}_3$, herein termed HDT) via incubation in an array of glass microcapillaries. Reference cantilevers were coated with the nonionizable HDT, which has an identical chain length and reportedly¹⁵ similar packing density to MHA but differs in the terminal methyl group (Figure 1A). The modified cantilever array was then mounted in a sealed liquid cell. A home-built gravity flow system was developed to control the exchange of up to six different sodium phosphate solutions via an automated valve (Figure 1B). All signals were acquired under an average liquid flow rate of $150 \pm 30 \mu\text{L}/\text{min}$. Variations in flow rate within this range were not found to substantially affect the equilibrated bending signals. The absolute deflection at the free-end of each cantilever Δz_{abs} was measured using a time-multiplexed optical detection system in different liquid environments (Scentris Veeco Instruments Inc., Santa Barbara, CA, see Materials and Methods). Herein we present raw data, without any baseline corrections. The bending signal was subsequently converted into a difference in surface stress between the upper and lower sides of the cantilever $\Delta\sigma_{\text{abs}}$, using the Stoney's equation¹⁶

$$\Delta\sigma_{\text{abs}} = \frac{1}{3} \left(\frac{t}{L} \right)^2 \frac{E}{1-\nu} \Delta z_{\text{abs}} \quad (1)$$

where L is the effective length of the cantilever going up to 500 μm , $t = 0.9 \mu\text{m}$ is the thickness, and $E/(1-\nu) = 181 \text{ GPa}$ is the ratio between the Young's modulus E and Poisson ratio ν of Si (100), which is invariant within the {100} planes.¹⁷ The differential surface stress $\Delta\sigma_{\text{diff}}^{\text{(MHA/HDT)}}$ specific to MHA ionization was calculated by subtracting the reference HDT absolute surface stress $\Delta\sigma_{\text{abs}}^{\text{(HDT)}}$ from the MHA absolute surface stress $\Delta\sigma_{\text{abs}}^{\text{(MHA)}}$, i.e., $\Delta\sigma_{\text{diff}}^{\text{(MHA/HDT)}} = \Delta\sigma_{\text{abs}}^{\text{(MHA)}} - \Delta\sigma_{\text{abs}}^{\text{(HDT)}}$. In this report, a positive absolute deflection cor-

(13) Raiteri, R.; Butt, H.-J.; Grattarola, M. *Electrochim. Acta* **2000**, *46*, 157–163.

(14) Fritz, J.; Baller, M. K.; Lang, H.-P.; Strunz, T.; Meyer, E.; Güntherodt, H.-J.; Delamarche, E.; Gerber, C.; Gimzewski, J. K. *Langmuir* **2000**, *16*, 9694–9696.

(15) Nuzzo, R. G.; Dubois, L. H.; Allara, D. L. *J. Am. Chem. Soc.* **1990**, *112*, 558–569.

(16) Stoney, G. G. *Proc. Roy. Soc. London, Ser. A* **1909**, *82*, 172–175.

(17) Brantley, W. A. *J. Appl. Phys.* **1973**, *44*, 534–535.

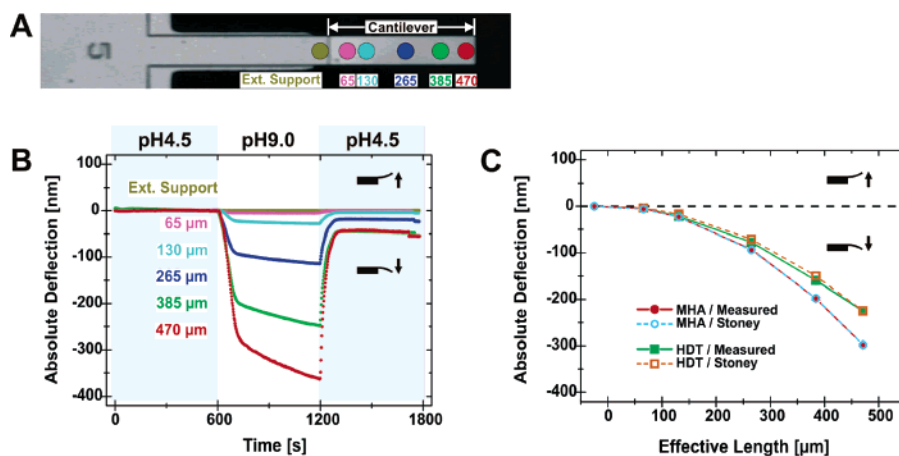


Figure 2. (A) Micrograph of a single cantilever to show the effective lengths investigated: extended support structure (dark yellow), 65 μm (magenta), 130 μm (cyan), 265 μm (blue), 385 μm (green), and 470 μm (red). (B) Raw absolute signals associated with pH 4.5/9.0/4.5 sodium phosphate cycle taken at the given effective lengths on a MHA-coated cantilever. (C) Equilibrium pH 4.5/9.0/4.5 MHA (circles) and HDT (rectangles) absolute signals as a function of the effective length (solid symbols and solid line), superimposed on expected values according to the Stoney's equation (symbols and dashed lines). Note that owing to the small standard errors for these measurements, the error bars associated with each data point are not visible in (C).

responds to the upward bending of the cantilever due to a tensile surface stress and a negative absolute deflection to the downward bending of the cantilever due to a compressive surface stress, in accord with the common sign convention.¹⁸

Results

Characterization of SAMs. Multiple arrays of eight identical silicon cantilevers were coated with a thin film of gold and functionalized with either MHA or HDT via incubation for 20 min in microcapillaries filled with 4 mM ethanolic thiol solutions. The resultant SAMs were characterized by contact angle goniometry, spectroscopic ellipsometry and X-ray photoelectron spectroscopy. Given the miniaturized geometry of cantilevers, characterization of the SAMs was performed instead on silicon wafers which had been functionalized in parallel to silicon cantilevers. The typical advancing contact angle of water on HDT SAMs was found to be $111 \pm 2^\circ$, whereas a water droplet was observed to completely wet MHA SAMs with a sessile contact angle of $<10^\circ$ under ambient atmosphere. Spectroscopic ellipsometry revealed SAM film thicknesses of $19 \pm 2 \text{ \AA}$ and $20 \pm 2 \text{ \AA}$ respectively, in agreement with the theoretical expectation based on an all-*trans* chain with a 30° tilt angle.¹² High-resolution X-ray photoelectron spectra of the carbon 1s region (Supporting Information) were also found to be in excellent agreement with reported data on monolayers prepared via 24 h incubation.^{12,15}

Homogeneity of Surface Stress Action along the Cantilever. The bending signals of an array of eight microcantilevers were monitored using a time-multiplexed optical detection scheme as the pH of sodium phosphate solution at a constant ionic strength of $\mu = 0.1$ was cycled between pH 4.5 and 9.0. To investigate the homogeneity of pH-triggered surface stress action along the long axis of the micromechanical cantilever, initial experiments measured the bending signal at different positions on the beam structure, i.e., starting from the 5.9 μm thick extended support to the 0.9 μm thick cantilever at the effective lengths 65, 130, 265, 385, and 470 μm by moving the laser position, as shown in Figure 2A. To ensure that the laser

spots were aligned at equivalent positions for all cantilevers, heating tests that rely on the bimetallic effect were first performed at each effective length prior to the pH measurements. Figure 2B shows the raw bending signals for a typical MHA-coated cantilever upon switching between pH 4.5/9.0/4.5 liquid environments. It can be seen that at pH 4.5, the bending signal was stable under constant liquid flow. Upon switching to pH 9.0, where the carboxylic acid terminating SAMs are expected to be ionized, the cantilever bent downward corresponding to a compressive surface stress. When the aqueous environment was switched back to pH 4.5, the bending signal returned toward the zero-stress baseline. The pH-triggered change in cantilever bending profile shown in Figure 2C was determined by plotting the equilibrium pH 9.0 bending signal at each effective length (solid symbols and solid lines). Thereby each data point represents the mean and standard error of the *deprotonation* $\Delta z_{\text{abs}} (\text{pH } 4.5/9.0)$ absolute bending signals associated with the switch from pH 4.5 to 9.0, and *protonation* $\Delta z_{\text{abs}} (\text{pH } 9.0/4.5)$ absolute bending signals associated with the switch from pH 9.0 back to 4.5, taken on two MHA- (red circles in Figure 2C) and two HDT-coated (green rectangles in Figure 2C) cantilevers, respectively. Both deprotonation and protonation reactions refer to the reference pH 4.5, i.e., both the deprotonation and protonation absolute bending signals are determined by subtracting the signal observed at pH 4.5 from the signal observed at pH 9.0. The absolute deflection is attributed to a combination of surface stress induced by the *specific* ionization of MHA and *nonspecific* influences including reactions occurring at non-functionalized sites on the gold and at silicon oxide underside of the cantilever, changes in refractive index or in the temperature of the aqueous environment. These nonspecific effects will affect both MHA and HDT signals to the same extent and are eliminated by taking a differential measurement (MHA minus HDT signal). The measured bending profile was then superimposed on the expected profile of MHA (light blue hollow circles and dashed lines in Figure 2C) and HDT (orange hollow rectangles and dashed lines in Figure 2C) signals according to the Stoney's equation (eq 1), respectively, by assuming that the surface stress measured at the maximal effective length of 470

(18) Müller, P.; Saül, A. *Surf. Sci. Rep.* **2004**, *54*, 157–258.

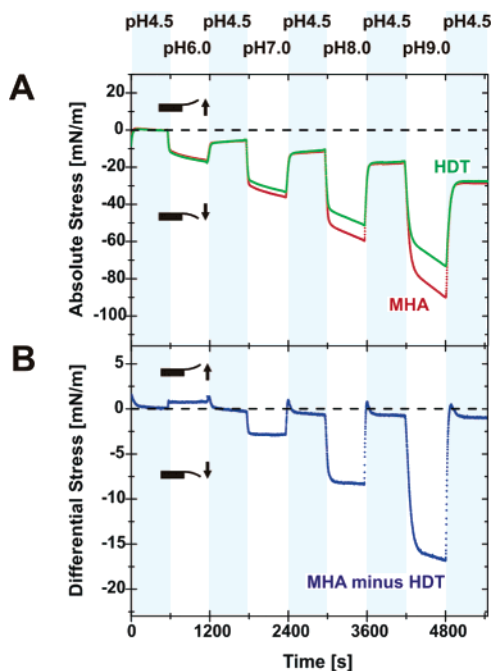


Figure 3. (A) Absolute surface stress signals for MHA and HDT cantilevers as a function of sodium phosphate solution pH at constant ionic strength $\mu = 0.1$. (B) Differential signal (MHA minus HDT).

μm acts homogeneously at the cantilever surface. As shown in Figure 2C, the measured signals were found to be in an excellent agreement with the expected values, indicating a uniform surface stress generation along the long axis of the cantilever.

Surface Stress Titration. To investigate the micromechanical bending signal as a function of increasing pH of sodium phosphate solution at a constant ionic strength of $\mu = 0.1$, the aqueous environment was cycled between pH 4.5, 6.0, 4.5, 7.0, 4.5, 8.0, 4.5, 9.0, 4.5 under constant liquid flow. The absolute bending signal of a typical MHA (red in Figure 3A) and HDT (green in Figure 3A) coated cantilever is shown in Figure 3A. Alternate injections of pH 4.5 phosphate solution served as an important control to investigate the reversibility of deprotonation/protonation reactions, since at this pH the majority of carboxylic acid groups have been assumed to be protonated. Upon injecting increasingly higher pH solutions (6.0, 7.0, 8.0, 9.0) it can be seen that both MHA and reference HDT cantilevers bent downward corresponding to a compressive absolute surface stress (cantilever bending away from the gold coating, as illustrated in Figure 1A). The corresponding differential signals specific to the MHA surface ionization are shown in Figure 3B. It can be seen that upon switching from pH 4.5 to 6.0 the difference in absolute bending between the MHA cantilever and HDT cantilever was positive reaching an equilibrium signal $\Delta z_{\text{diff}} (\text{pH } 4.5/6.0) = 2.7 \text{ nm}$ under constant liquid flow, which corresponds to a tensile differential stress $\Delta \sigma_{\text{diff}} (\text{pH } 4.5/6.0) = 0.6 \text{ mN/m}$. When the pH was cycled back to pH 4.5, the differential signal was observed to return to the baseline, $\Delta \sigma_{\text{diff}} (\text{pH } 6.0/4.5) = 0.7 \text{ mN/m}$. Upon switching to more alkaline pH environments, the resulting differential signals rendered increasingly more compressive. The estimated mean differential stress and standard error¹⁹ resulted from a single cantilever array comprising three MHA- and three HDT-coated cantilevers, three pH cycles, and deprotonation/protonation reactions was estimated to be $\Delta \sigma_{\text{diff}} (\text{pH } 4.5/6.0/4.5) = +0.9 \pm 0.3$

mN/m at pH 6.0, $\Delta \sigma_{\text{diff}} (\text{pH } 4.5/7.0/4.5) = -2.4 \pm 0.6 \text{ mN/m}$ at pH 7.0, $\Delta \sigma_{\text{diff}} (\text{pH } 4.5/8.0/4.5) = -7.7 \pm 0.6 \text{ mN/m}$, at pH 8.0, and $\Delta \sigma_{\text{diff}} (\text{pH } 4.5/9.0/4.5) = -14.5 \pm 0.5 \text{ mN/m}$ at pH 9.0. The observed differential signals are in a good agreement with Fritz et al.,¹⁴ however whereas they reported a compressive stress of approximately -2 mN/m at pH 6.0, our investigations reveal a tensile surface stress of $+0.9 \pm 0.3 \text{ mN/m}$.

Statistical Analysis. To probe the reproducibility of the tensile differential stress observed at pH 6.0, four separate cantilever arrays comprising a total of 19 cantilevers were exposed to successive injections of pH 4.5/6.0/4.5 sodium phosphate solutions. The development of a semiautomated evaluation method was found to be essential for the analysis of large data sets with minimal user bias. Briefly, the software generated a linear fit to the raw data acquired in each liquid environment to determine the absolute deprotonation/protonation signals after equilibration. Analysis of variance (ANOVA)²⁰ was performed thereafter to investigate the sources of variation in these signals. More details of the evaluation method, including the measured deprotonation/protonation absolute stress signals and the statistical model, are given in the Supporting Information.

The main finding of the between-cantilever comparison was that the mean differential stress was tensile, $+1.2 \pm 0.3 \text{ mN/m}$ ($p < 0.0005$). Although there was no evidence of variation between the differential signals across four cantilever arrays ($p = 0.4$), clear evidence of variation was found in the corresponding absolute stress ($p < 0.0005$), thus emphasizing the importance of differential stress measurements. The total between-cantilever variance was estimated to be $0.56 (\text{mN/m})^2$.

The *effective* variance of the within-cantilever measurement error was estimated to be only $0.006 (\text{mN/m})^2$. This allowed us to probe very small changes in surface stress, which would otherwise be masked by the approach commonly used to evaluate differential measurement.^{1,2,5,6,14} The small *effective* within-cantilever variance revealed an estimated mean difference, in the protonation minus deprotonation differential stress signal, of $+0.18 \pm 0.05 \text{ mN/m}$ ($p = 0.01$). This hysteresis showed no evidence of variation between the four cantilever arrays ($p = 0.2$), but again clear evidence of variation was found in the corresponding absolute stress ($p < 0.0005$).

Our work confirms the importance of differential measurements. Multiple observations on the same cantilever, on different cantilevers and different cantilever arrays allow more precise estimation of the generated surface stress. Ongoing experimental and statistical work will further investigate the various sources of variation of both between- and within-cantilever effects, including successive cycles and measurement order.²¹

Effect of Ionic Strength. Building upon the titration studies described above, our next experiments probed the differential bending response to different ionic strengths of sodium phosphate aqueous solutions. Figure 4A,B shows typical absolute and differential measurements, respectively, taken on a cantilever array comprising three MHA and four HDT coated

(19) Throughout this manuscript, the reported surface stress value corresponds to estimated mean and estimated standard error determined by appropriate ANOVAs based on a statistical model. See Supporting Information for details.

(20) Montgomery, D. C. *Design and Analysis of Experiments*, 6th ed.; Wiley Press: Hoboken, NJ, 2005.

(21) Watari, M.; Galbraith, J.; Horton, M. A.; McKendry, R. A. *Manuscript in preparation*.

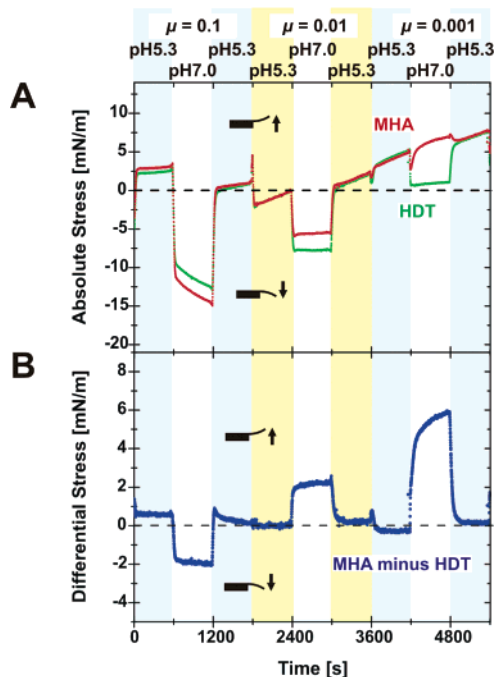


Figure 4. (A) Absolute and (B) differential surface stress change associated with alternate injection of pH 5.3 and 7.0 sodium phosphate solutions with decreasing ionic strengths, $\mu = 0.1, 0.01,$ and 0.001 .

cantilevers. The cantilever array was exposed to an alternate injection of pH 5.3 and 7.0 sodium phosphate solutions prepared at the ionic strengths $\mu = 0.1, 0.01,$ and 0.001 . Statistical analysis of the differential stress found that in-plane MHA forces were dependent upon ionic strength when the pH was varied between 5.3 and 7.0. The 5.3/7.0 pH switch at the highest and default ionic strength of $\mu = 0.1$, gave a compressive differential surface stress of -2.6 ± 0.8 mN/m. However, when the ionic strength was reduced by an order of magnitude to $\mu = 0.01$, the pH 5.3/7.0 differential bending response was observed to invert to give a tensile differential surface stress signal of $+2.8 \pm 0.6$ mN/m. Upon further reducing the ionic strength to $\mu = 0.001$, the tensile signal increased to $+5.7 \pm 0.3$ mN/m.

Effect of Different Counter- and Co-ions in Solution. To further investigate the role of the aqueous environment on MHA surface stress, our studies extended to probe the effect of different counter- and co-ions. The surface stress triggered by the pH 4.5/9.0/4.5 switch (at constant ionic strength $\mu = 0.1$) was compared for two different cations: sodium and ammonium phosphate ($\text{Na}^+, \text{NH}_4^+$). Then the influence of different anions was probed by comparing pH 9.0 ammonium chloride and ammonium nitrate ($\text{Cl}^-, \text{NO}_3^-$) in addition to the ammonium phosphate ($\text{H}_x\text{PO}_4^{-(3-x)}$). Figure 5 shows the differential signal when the MHA/HDT cantilever array was exposed to the following series of aqueous environments; pH 4.5/9.0/4.5 sodium phosphate ($\text{Na}_{3-x}\text{H}_x\text{PO}_4$); pH 4.5/9.0/4.5 ammonium phosphate ($(\text{NH}_4)_{3-x}\text{H}_x\text{PO}_4$); pH 9.0 ammonia/ammonium chloride ($\text{NH}_3^+/\text{NH}_4\text{Cl}$); pH 4.5 ammonium phosphate, pH 9.0 ammonia/ammonium nitrate ($\text{NH}_3^+/\text{NH}_4\text{NO}_3$); pH 4.5 ammonium phosphate, and pH 4.5 sodium phosphate. The statistical analysis of differential signals revealed that the bending response is not only dependent on the pH or the ionic strength but also on the ion species present in the aqueous environment. Figure 5 shows that upon switching the pH between 4.5 and 9.0 sodium phosphate solutions, a compressive differential stress of -13.6

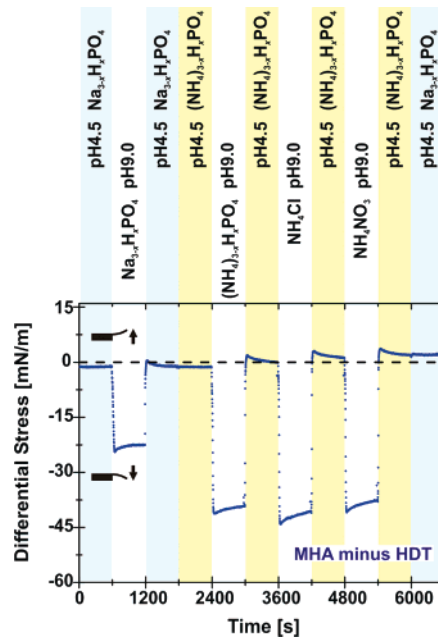


Figure 5. Typical differential measurement to probe the effect of counter- and co-ions. The signal was obtained upon alternate injection of $\mu = 0.1$ pH 4.5/9.0/4.5 $\text{Na}_{(3-x)}\text{H}_x\text{PO}_4$, pH 4.5/9.0/4.5 $(\text{NH}_4)_{(3-x)}\text{H}_x\text{PO}_4$, pH 9.0 $\text{NH}_3^+/\text{NH}_4\text{Cl}$, pH 4.5 $(\text{NH}_4)_{(3-x)}\text{H}_x\text{PO}_4$, pH 9.0 $\text{NH}_3^+/\text{NH}_4\text{NO}_3$, pH 4.5 $(\text{NH}_4)_{(3-x)}\text{H}_x\text{PO}_4$, and pH 4.5 $\text{Na}_{(3-x)}\text{H}_x\text{PO}_4$.

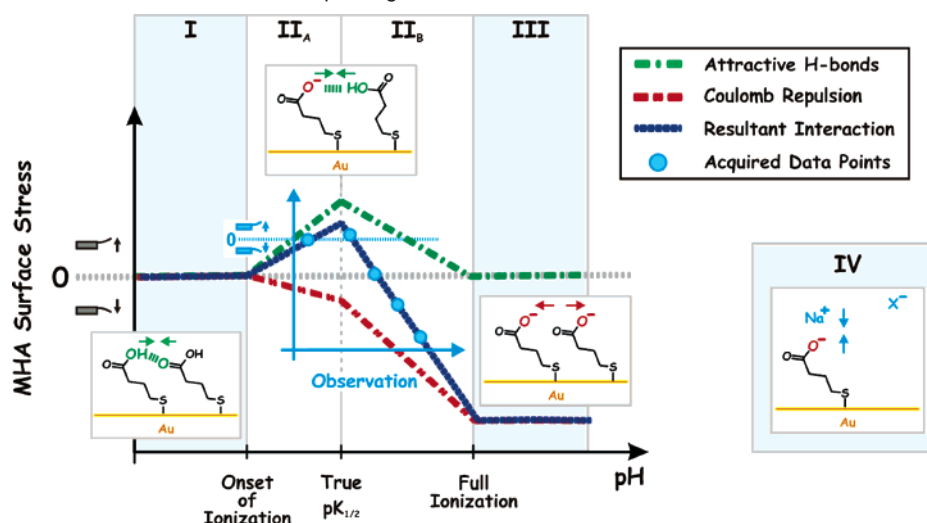
± 3.9 mN/m was observed. This is in agreement with the data shown in Figure 3 and served as another important control measurement. When the solution was switched from pH 4.5 sodium phosphate to pH 4.5 ammonium phosphate, a slightly tensile signal of $+1.7 \pm 0.5$ mN/m was detected, though ANOVA showed that there was no strong evidence for this effect ($p = 0.08$). Whereas when the aqueous solution was switched between pH 4.5 and 9.0 ammonium phosphate, the in-plane surface forces increased to -47.2 ± 4.8 mN/m. The magnitude of the compressive differential stress observed in the ammonium phosphate solution was found to be comparable to the signal of ammonium chloride -50.4 ± 5.2 mN/m and ammonium nitrate -47.5 ± 5.1 mN/m. A common reference pH 4.5 ammonium phosphate solution was employed for these anions.

Discussion

Our findings demonstrate the unique capability of multiple cantilever arrays to detect specific in-plane mechanochemical forces induced by the ionization reactions of the MHA SAMs in aqueous environments. Although in-plane force titration studies showed that absolute cantilever bending can arise from a combination of both specific effects and nonspecific influences, including temperature, changes in refractive index, and reactions occurring on the silicon oxide underside, differential measurements with *in situ* reference cantilevers were found to be essential to probe chemically specific bending signals. HDT was chosen as a reference SAM because it has an identical chain length to MHA, a similar reported packing density¹⁵ and no ionizable groups. In addition to a reference cantilever, the reference pH 4.5 sodium phosphate solution was used, because the majority of carboxylic acid groups are assumed to be protonated at this pH.¹⁴

To probe the homogeneity of stress action, the bending profile was measured along the long axis of the micromechanical

Scheme 1. MHA Surface Ionization State in Different pH Regimes



cantilever. Upon the alternate injection of pH 4.5/9.0 sodium phosphate solutions, both MHA and HDT were found to exhibit a constant cantilever curvature, in agreement with the Stoney's equation (eq 1).¹⁶ The validity of this equation has recently been subject to much debate in the literature.^{22–26} However, in this literature, critical parameters varied including the specific experimental or modeled system under investigation (bimetallic heat transduction or SAM formation), the environment (vacuum, air, or liquid), cantilever geometry and material. These factors may, at least in part, explain the discrepancies in the direction and homogeneity of the reported bending signals. In contrast, here we have optimized the surface chemistry and fluid flow to ensure the rapid and homogeneous exchange of different liquid environments to induce specific chemical reactions at the cantilever solid–liquid interface. Under these optimized conditions, our findings show that the surface stress profile along the long axis of the cantilever beam induced by SAM ionization can be accurately described by the Stoney's equation, indicating a homogeneous surface stress transduction.

The development of an automated raw data evaluation algorithm was found to be essential to evaluate large data sets with minimal user bias. Moreover, the analysis of variance model for the multiple cantilever array data allowed us to estimate the differential stress and its variance, and, importantly, to deconvolute the different sources of variability that result from multiple measurements on separate cantilever arrays. It is important to note that although a number of groups have reported surface stress measurements on a range of different chemical and biological systems, to date there has been no detailed study of the statistical variability of measurements and yet this is essential for all potential sensing applications. Here we show that the development of a statistical model for the cantilever array data is particularly important to probe the small tensile surface stress observed at pH 6.0, i.e., $+1.2 \pm 0.3$ mN/m. Previous pH titration surface stress studies on acid-terminating SAMs have varied widely and are largely limited due to the use of single cantilever measurements.¹³ Our findings

are in good agreement with the differential measurements of Fritz et al.¹⁴ for $\text{pH} > 7.0$ but differences became more prominent at low pH, where herein the sign of small surface stress inverted to give a tensile mean differential stress. Fritz reported a small compressive surface stress of approximately -2 mN/m at pH 6.0, however no detailed statistical analysis was performed to assess the statistical significance of this observation.¹⁴ In contrast, here, 38 measurements were made on a total of 19 cantilevers distributed on 4 separate cantilever arrays and analyzed via an ANOVA based on a statistical model. Differences in surface stress to published data may arise due to sample preparation, for example molecular packing and gold morphology. In this study, SAMs were characterized using XPS, ellipsometry, and contact angle goniometry (Supporting Information) and were shown to be in excellent agreement with high-quality SAMs reported in published data.^{12,15}

To rationalize the cantilever bending response as a function of the increasing pH of sodium phosphate aqueous solution, we propose a simple model comprising three distinct pH regimes determined by the ionization state of the carboxylic acid terminating SAM, as illustrated in Scheme 1. We will initially consider the three different pH regimes (I–III) in turn, and then extend our discussion to consider the influence of solution-phase ions on in-plane MHA forces (IV).

In the first regime at low pH, the MHA SAM is assumed to be fully protonated and the in-plane interaction is governed by the formation of attractive neutral hydrogen bonds $\text{COOH} \cdots \text{COOH}$ (Scheme 1, I). With increasing pH, the second regime starts with the onset of ionization to yield a negatively charged carboxylate ion and then extends to the pH at which full ionization of every surface acid group is achieved (Scheme 1, II). This regime is further subdivided into two parts: from the onset of ionization to the $\text{pK}_{1/2}$ is termed IIA, whereas from the $\text{pK}_{1/2}$ to full ionization is IIB. In IIA, as the pH is increased, adjacent deprotonated and protonated carboxylic acid groups can form in-plane attractive ionic hydrogen bonds $\text{COO}^- \cdots \text{COOH}$. By definition, the number of ionic H-bonds formed will become maximal at the surface $\text{pK}_{1/2}$. Whereas in IIB as the pH is increased above the surface $\text{pK}_{1/2}$, there will be electrostatic repulsion between adjacent deprotonated carboxylic acid groups $\text{COO}^- \cdots \text{COO}^-$. However, in IIA and IIB, the resultant in-plane force (blue short dotted line) will be a superposition of both

(22) Jeon, S.; Thundat, T. *Appl. Phys. Lett.* **2004**, *85*, 1083–1084.

(23) Mertens, J.; Alvarez, M.; Tamayo, J. *Appl. Phys. Lett.* **2005**, *87*, 234102.

(24) Rasmussen, P. A.; Hansen, O.; Boisen, A. *Appl. Phys. Lett.* **2005**, *86*, 203502.

(25) Klein, C. A. *J. Appl. Phys.* **2000**, *88*, 5487–5489.

(26) Sader, J. E. *J. Appl. Phys.* **2001**, *89*, 2911–2921.

the attractive ionic hydrogen bonding (green dash-dot-dashed line) and Coulomb repulsion (red dash-dot-dot-dashed line) as shown in Scheme 1. In the third distinct pH regime of this model, the SAM is fully ionized and the resultant force is governed by electrostatic repulsion (Scheme 1, III).

The model in Scheme 1 can be applied to the experimental surface stress profile of MHA measured herein, although our data constitute an observation window onto the *true* surface stress titration behavior. This is illustrated by the relative coordinate system of the window in Scheme 1 (blue axes) with respect to the coordinate system of the model (black axes). At the lower pH limit of 4.5 used herein, the largest population of surface carboxylic acid groups is assumed to be protonated and thus served as the reference zero stress state for all cantilever measurements. We show that the magnitude of in-plane attractive forces reached a maximum at pH 6.0, and with increasing pH, the differential signal was found to invert due to increasingly repulsive compressive differential stress at 7.0, 8.0, and 9.0. It should be noted that the magnitude of the differential surface stress observed in these measurements does not saturate at 4.5 and 9.0, suggesting that our observation window falls in the intermediate pH regime II.²¹ Because the bond strength of a neutral and ionic hydrogen bond reportedly²⁷ differs by an order of magnitude, 5 and 29 kcal/mol, respectively, the MHA tensile surface stress is expected to be maximized at the *true* surface $pK_{1/2}$. We therefore propose that the tensile differential stress of $+1.2 \pm 0.3$ mN/m observed at pH 6.0 reflects an enhanced ionic hydrogen bond interaction. This maximum observed tensile stress should be considered as an *apparent* $pK_{1/2}$ under these experimental conditions, i.e., $\mu = 0.1$ sodium phosphate solution. The compressive surface stress observed at pH 7.0 relative to pH 4.5 indicates that the *true* surface $pK_{1/2}$ lies within the range pH 4.5–7.0. The measured apparent surface $pK_{1/2}$ implies an alkaline shift compared to the pK_a of carboxylic acid groups in bulk solution phase, for example formic acid 3.75.²⁸ This alkaline shift has been reported in the literature^{29–37} and may be attributed to Coulombic interactions between the neighboring deprotonated carboxylic acid groups, dipole–dipole interactions between the carboxylic acid groups and the aqueous phase, or the dielectric contrast between the hydrocarbon monolayer ($\epsilon_{\text{Alkanes}} \approx 2$) and the aqueous phase ($\epsilon_{\text{H}_2\text{O}} \approx 80$)²⁸ promoting ion migration toward the lower dielectric.²⁹ Yet, whereas previous titration studies such as chemical force microscopy probed the out-of-plane forces acting between two approaching surfaces coated with carboxylic acid terminating SAMs,^{31–33} this technique cannot probe in-plane forces and moreover is

limited by the liquid confinement effects. Contact angle goniometry has detected an increase in the hydrophobicity of the carboxylic acid terminating SAMs associated with the formation of in-plane hydrogen bonds.³⁰ However the applicability of this technique in determining the surface free energy has been subject to debate,^{12,29,30,38} as the nature of the three-phase boundary is yet not well understood. Therefore, even though different techniques have been used to investigate the titration behavior of surface tethered carboxylic acid groups, the cantilever array experiments herein represent a unique approach to probe directly the chemically specific in-plane forces generated at the liquid/solid interface. It is important to appreciate that the differential surface stress measurements using free-standing cantilevers reported herein offer the first direct measure of the in-plane attractive forces exerted by the formation of ionic hydrogen bonds associated with the surface $pK_{1/2}$. By assuming the reported packing density of 21.4 Å² per alkanethiol,³⁹ the observed tensile differential MHA surface stress of 1.2 ± 0.3 mN/m at the apparent $pK_{1/2}$ translates into an average in-plane attractive force of 1 pN exerted by each pair of adjacent MHA molecules, although this estimate does not consider inherent roughness of the surface but only the geometry of the cantilever.

However, the simple model of in-plane differential stress generation in the intermediate pH regime based upon the attractive hydrogen bond interaction and repulsive coulomb interaction should be applied with caution. Although it appears intuitive that the observed compressive differential surface stress at pH ≥ 7.0 primarily arises from the electrostatic repulsion between the adjacent deprotonated carboxylic acid groups, our investigations reveal the important role of the counterions and co-ions present in the aqueous environment (Scheme 1, IV). It was expected that at pH 7.0, a decrease in ionic strength from $\mu = 0.1, 0.01$ to 0.001 would increase the Debye screening length and so in turn, increase the in-plane electrostatic repulsion giving rise to an increased compressive differential surface stress. However, herein we report the opposite effect: as the ionic strength was decreased, the compressive differential stress signal at $\mu = 0.1$ was observed to invert and became increasingly tensile at lower ionic strengths of $\mu = 0.01$ and 0.001. At present, the relation between the ionic strength and MHA surface stress is not well understood. Indeed, one must not only consider the in-plane attractive and repulsive interaction between carboxylic acid groups but also the pH dependent ion concentration of the bulk sodium phosphate solution ions (described by the Henderson–Hasselbalch equation), and the interaction of solution-phase ions at the MHA/liquid interface.

The important role of solution ions on MHA in-plane forces was highlighted by the results shown in Figure 5 (Scheme 1 IV). A comparison of the pH 4.5/9.0 switch for two different monovalent cations, Na⁺ and NH₄⁺, both probed in phosphate solution at a constant ionic strength of $\mu = 0.1$, found that the in-plane surface forces were more than 2-fold larger for ammonium than for sodium cations, whereas statistical analysis of three different anion species at pH 9.0 (HPO₄²⁻, Cl⁻, and NO₃⁻) found the mean compressive differential stress signals were not distinguishable within the associated standard errors, estimated by an ANOVA. These findings show the significant effect of different cations on the magnitude of MHA in-plane

(27) Meot-Ner, M.; Elmore, D. E.; Scheiner, S. *J. Am. Chem. Soc.* **1999**, *121*, 7625–7635.

(28) *CRC Handbook of Chemistry and Physics*, 86th ed.; CRC Press: Boca Raton, FL, 2005.

(29) Holmes-Farley, S. R.; Reamey, R. H.; McCarthy, T. J.; Deutch, J.; Whitesides, G. M. *Langmuir* **1985**, *1*, 725–740.

(30) Lee, T. R.; Carey, R. I.; Biebuyck, H. A.; Whitesides, G. M. *Langmuir* **1994**, *10*, 741–749.

(31) Vezenov, D. V.; Noy, A.; Rozsnyai, L. F.; Lieber, C. M. *J. Am. Chem. Soc.* **1997**, *119*, 2006–2015.

(32) Van der Vegte, E. W.; Hadziioannou, G. *J. Phys. Chem. B* **1997**, *101*, 9563–9569.

(33) Smith, D. A.; Wallwork, M. L.; Zhang, J.; Kirkham, J.; Robinson, C.; Marsh, A.; Wong, M. *J. Phys. Chem. B* **2000**, *104*, 8862–8870.

(34) Wang, J.; Frostman, L. M.; Ward, M. D. *J. Phys. Chem.* **1992**, *96*, 5224–5228.

(35) Schweiss, R.; Welzel, P. B.; Werner, C.; Knoll, W. *Langmuir* **2001**, *17*, 4304–4311.

(36) Gershevit, O.; Sukenik C. N. *J. Am. Chem. Soc.* **2004**, *126*, 482–483.

(37) Konek, C. T.; Musorafitij, M. J.; Al-Abadleh, H. A.; Bertin, P. A.; Nguyen, S. T.; Geiger, F. M. *J. Am. Chem. Soc.* **2004**, *126*, 11754–11755.

(38) Fowkes, F. M. *Ind. Eng. Chem.* **1964**, *56*, 40–52.

(39) Strong, L.; Whitesides, G. M. *Langmuir* **1988**, *4*, 546–558.

forces at pH 9.0. One might suggest that the smaller sodium cations are able to screen the repulsive forces between negatively charged COO^- groups more efficiently than larger ammonium cations, upon the basis of literature ionic crystal radius of 0.95 and 1.48 Å, respectively.⁴⁰ However, the corresponding hydrated radii are similar, 3.58 and 3.31 Å for sodium and ammonium cation, respectively.⁴⁰ Future work will involve a systematic study of different mono-, di-, and trivalent cations to investigate the effects of ion size and hydration on the generation of deprotonation induced MHA in-plane forces.²¹

Our findings are of substantive importance, not only for cantilever studies but for all investigations of charged solid surfaces exposed to aqueous environments, where the medium is often considered as merely “background”. Titration studies have previously been performed in a wide range of environments with different counterions, co-ions, in buffered or non-buffered solutions. Our measurements show that the in-plane surface forces are highly sensitive to pH, ionic strength, plus different ion species present in solution, demonstrating that the published literature should be interpreted with caution. Although the work presented herein is focused on chemically well-defined SAMs, these findings will also be important for our understanding of in-plane forces of biological interfaces and membranes.

Conclusion

To conclude, systematic differential surface stress titration measurements have shown the sensitivity to detect attractive in-plane forces associated with ionic hydrogen bond formation at the apparent surface $\text{p}K_{1/2}$ and the electrostatic repulsion between deprotonated carboxylic acid groups at elevated pH. Our studies reveal the dominant role of counterions in the aqueous environment in the generation of in-plane mechanochemical forces, which controls both the magnitude and direction of cantilever motion. These surface in-plane forces will become increasingly important as the dimensions of the solid shrink down to the nanometer scale. Understanding the complex dynamic three-phase equilibrium between hydrophilic and hydrophobic SAMs, interfacial ions, water molecules, and the bulk solution presents a challenging goal for both experiment and theory. Ongoing experiments will probe the ionic strength dependence over the full pH range, different monovalent and divalent ions²¹ plus the influence of SAM chain length and terminal groups, including OH and NH_2 functionalities.²¹ These findings will provide new insights into the fundamental mechanisms of surface stress generation, which have broad implications in the study of biochemical interfaces from molecular thin films to cellular membranes.

Materials and Methods

Preparation of Cantilevers and Silicon Wafers. Cantilever arrays were fabricated by IBM Research Laboratory, Rüschlikon, Switzerland, and purchased from Veeco Instruments. The nominal dimension of each Si (100) cantilever was 500 μm in length, 100 μm in width, and 0.9 μm in thickness. Cantilever arrays were first cleaned with freshly prepared piranha solution (at ratio 1:1 H_2SO_4 and H_2O_2 —CAUTION: Piranha solution is hazardous and can cause explosions or severe skin burns if not handled with great care) for 20 min and rinsed thoroughly in deionized water. Second, the arrays were immersed into a solution comprising $\text{H}_2\text{O}/\text{H}_2\text{O}_2/\text{NH}_4\text{OH}$ (at ratio 1:1:1) for 10 min and again rinsed thoroughly with deionized water. Finally, the arrays were rinsed

with pure ethanol and dried on a hotplate at 75 °C. Thereafter, cantilever arrays were evaporated on one side with a thin film of gold (E-beam evaporation, 20 nm Au with 2 nm Ti adhesion layer, BOC Edwards Auto 306, U.K.), at a base pressure $\sim 2 \times 10^{-7}$ mbar and an evaporation rate of 0.04 nm/s for Ti and 0.07 nm/s for Au, measured directly above the source. Freshly evaporated cantilevers were sealed under argon and functionalized within a few hours after the evaporation. Thereby the cantilevers were incubated in an array of eight glass microcapillaries filled in random order with either 4 mM HDT or MHA for 20 min and rinsed in pure ethanol and deionized water. Functionalized cantilevers were then mounted onto a spring clip and stored in an amber bottle filled with deionized water at room temperature until use.

X-ray Photoelectron Spectroscopy. Spectra were taken on a VG Scientific Sigma Probe Spectrometer equipped with an aluminum Al K_α source with 1486.6 eV line energy and approximate beam spot size of 400 μm^2 . The pressure in the chamber was 3×10^{-9} mbar. High-resolution carbon C (1s) spectra between 280 and 293 eV binding energies were acquired with a 40 eV pass energy and averaged over 50 scans, as well as survey spectra between 0 and 600 eV binding energies with 80 eV pass energy averaged over 2 scans.

Spectroscopic Ellipsometry. Ellipsometric thicknesses of the SAMs as well as the lower layers, i.e., from top Au, Ti, and SiO_2 , were determined with a J.A. Woollam Variable Angle Spectroscopic Ellipsometer (VASE) using wavelengths between 300 and 1000 nm, a step interval of 10 nm, and at angles 65°, 70° and 75°.

Contact Angle Goniometry. Contact angles were probed in air with a Krüss DSA10 contact angle goniometer. The silicon wafer pieces coated with MHA SAM were completely wetted by water, whereas for HDT coated samples, a typical advancing angle of 111° was measured using an initial volume of 15 μL and injection rate of 8 $\mu\text{L}/\text{min}$.

Preparation of Aqueous Solutions. Mono- and dibasic sodium phosphate salts (0.1 M) were dissolved in ultrapure water (18.2 M Ω -cm resistivity, Millipore Co., Billerica, MA) and diluted according to the pH values 4.5, 6.0, 7.0, 8.0, and 9.0 to maintain a constant ionic strength of $\mu = 0.1$. The ionic strengths were calculated by assuming the literature $\text{p}K_a$ values for the phosphoric acid.²⁸ The pH value was measured using a commercial pH meter (Mettler-Toledo Ltd., Leicester, U.K.). Similarly, the pH 5.3 and 7.0 sodium phosphate $\text{Na}_{(3-x)}\text{H}_x\text{PO}_4$ aqueous solutions at three different ionic strengths of $\mu = 0.1, 0.01,$ and 0.001 were prepared by diluting the mono- and dibasic phosphate solution. After adjusting the pH values, the solutions were filtered using 0.2 μm filters (Millipore). The pH 4.5 and 9.0 ammonium phosphate $(\text{NH}_4)_{(3-x)}\text{H}_x\text{PO}_4$ aqueous solutions at $\mu = 0.1$ were prepared following the equivalent protocol used for the sodium phosphate solutions. Phosphoric acid H_3PO_4 and ammonium hydroxide NH_4OH , respectively, at $\mu = 0.1$ were used to decrease and increase the pH value where necessary. The ammonia/ammonium chloride and nitrate buffers were prepared by adjusting the pH of the 0.1 M NH_4Cl and 0.1 M NH_4NO_3 aqueous solutions using 4.0 M ammonium hydroxide solutions to pH 9.0, respectively. By assuming the literature $\text{p}K_a$ value for the ammonia,²⁸ the resulting solutions had an ionic strength of $\mu = 0.1$. The solutions were then degassed via 30 min ultrasonication and saturated with argon thereafter. All chemicals were purchased from Sigma-Aldrich (Sigma-Aldrich Co., St. Louis, MO).

Instrument. The absolute bending of all eight cantilevers was monitored using the serial time multiplexed optical beam method with a single position sensitive detector (Scentris, Veeco Instruments Inc., Santa Barbara, CA). The functionalized cantilever array was mounted in a sealed liquid chamber with a volume of approximately 80 μL . The liquid cell and each aliquot of aqueous solutions were placed into the temperature controlled cabinet to allow for temperature equilibration for at least 12 h prior to each experiment. At the beginning of each measurement, the bimetallic effect of the gold-coated cantilevers was exploited to align the each laser spot onto the free-end of each cantilever on the array. This is important to ensure that the effective length of all

(40) Nightingale, E. R. *J. Phys. Chem.* **1959**, *63*, 1381–1387.

eight cantilevers is equivalent. Upon heating the entire liquid cell by 1 °C, all eight cantilevers were observed to bend downward due to the bimetallic effect and the relative standard deviation among the equilibrated absolute bending signals was maintained to less than 2%. Herein, a positive deflection signal is defined as a tensile surface stress whereas a negative signal correlates to compressive stress, in agreement with the common sign convention.¹⁸ The efficient exchange of liquids in the liquid cell was achieved with a home-built gravity flow microfluidics system. Care was taken to investigate the influence of liquid flow rate during gravity flow on surface stress signal. Whereas the kinetics of bending signal was indeed found to depend on differences in flow rate, the equilibrium differential signal was found not to be substantively affected by flow rate under the conditions investigated herein. LabView (National Instruments Co., Austin, TX) software was implemented to automate the alternate flow of different pH sodium phosphate solutions via a 6-way valve (Serial MVP, Hamilton, Reno, NV). All signals were acquired under a liquid flow rate of $150 \pm 30 \mu\text{L}/\text{min}$ at the beginning of a measurement, which decreased at a constant rate of $0.25 \pm 0.03 \mu\text{L}/\text{min}$ during the measurements.

Acknowledgment. We thank Dr. Emmanuel Delamarche for thiols and IBM Rüschlikon for cantilever preparation facilities,

Dr. Jiayun Zhang (University of Basel), Dr. Alexander Bietsch (OC Oerlikon Balzers Ltd.), Dr. Joseph Ndieyira, and Dr. Christian Riener (UCL) for useful discussions. We also thank the IRC in Nanotechnology (Cambridge, UCL and Bristol), the Royal Society (R.McK. is a Royal Society Dorothy Hodgkin Research Fellow), BBSRC, The Wellcome Trust (M.A.H.), Overseas Research Students Award (M.W.), Swiss Embassy London, and the Human Frontier Science Program for funding.

Note Added after ASAP Publication. Due to a production error, the version of this paper published ASAP on December 29, 2006, was not the fully corrected proof. The corrected version was published ASAP on January 8, 2007.

Supporting Information Available: Details of the data evaluation method including the statistical model and software. This material is available free of charge via the Internet at <http://pubs.acs.org>.

JA065222X

SUPPORTING INFORMATION

X-ray Photoelectron Spectroscopy.

Figure S1 shows high resolution X-ray photoelectron spectroscopy of carbon 1s region acquired for MHA (red) and HDT (green). The principal peak at 284.7 eV is characteristic for aliphatic hydrocarbons. The high binding energy peak in the MHA spectrum at 289.3 eV arises from the bond between an α -carbon and a carbonyl group. Our data are in excellent agreement with published work by Bain *et al.*¹².

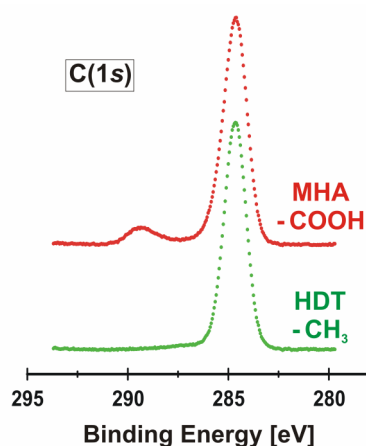


Figure S1: XPS carbon 1s spectra of MHA and HDT SAMs.

Evaluation Software and ANOVA Model.

The bending signals obtained from a cantilever array experiment are typically associated with multiple parameters such as separate cantilever arrays, an individual cantilever within the array, number of repeated measurements, and, in case of the pH experiments as presented herein, deprotonation or protonation reactions. The development of an appropriate evaluation algorithm by means of custom written software was found to be essential for a rapid analysis of large data sets with minimal user bias. Furthermore, a statistical model for an analysis of variance (ANOVA) was developed to estimate and to decompose the overall variability resulting from multiple

measurements into different components. The software used to evaluate the raw signals was written in IDL 6.0 (ITT Visual Information Solutions Co., Boulder, CO, U.S.A.), while the ANOVA was carried out using the statistical software package Minitab 13.32 (Minitab Inc., State College, PA, U.S.A.).

Consider the experiment performed in a single cycle of pH 4.5 / 6.0 / 4.5 sodium phosphate solutions at constant ionic strength of $\mu = 0.1$. This experiment involved a total of 19 cantilevers distributed on four separate cantilever arrays and coated with either HDT or MHA SAM. Two measurements were made on each cantilever, first the deprotonation absolute stress on switching from pH 4.5 to pH 6.0 and then the protonation absolute stress on switching back to pH 4.5. It should be noted that the following criteria were applied to discard an individual cantilever from the evaluation: (a) broken or visibly damaged cantilevers and (b) cantilevers which failed the heating test performed to align the SLD with the cantilever array. Both criteria were applied consistently throughout the data presented in this paper.

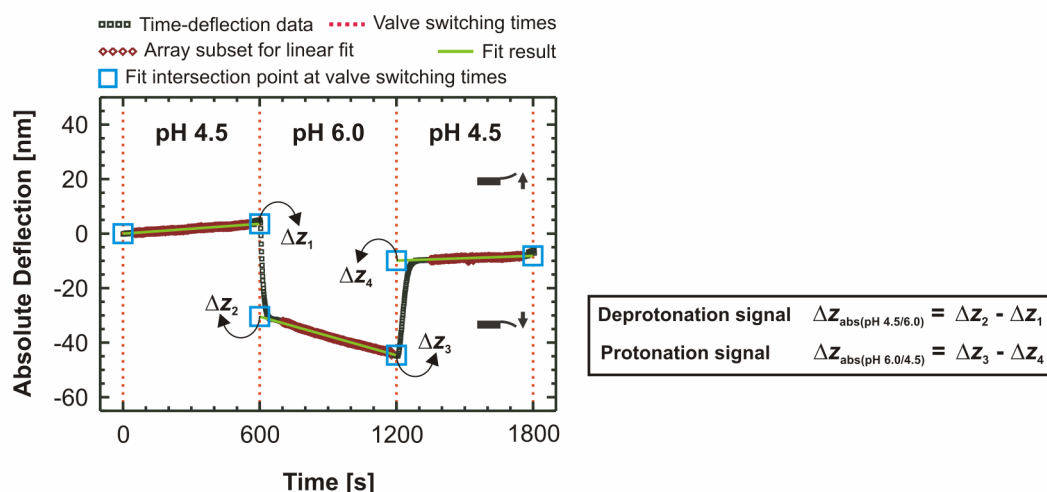


Figure S2: Semi-automated analysis of surface stress measurements.

The principle of the raw data evaluation algorithm is demonstrated in Figure S2 using an absolute signal (hollow black squares) acquired by switching from pH 4.5 / 6.0 / 4.5 sodium phosphate

solutions. A linear fit was applied to the raw time-deflection data points generated in each particular liquid environment. Subsequently, the fitted curves were extrapolated (green solid lines) to the onsets of liquid exchange (light blue hollow squares) to calculate the following two bending signals: (1) the *deprotonation* signal $\Delta z_{\text{abs (pH4.5/6.0)}}$ triggered by pH switch from 4.5 to 6.0 (2) and the *protonation* signal $\Delta z_{\text{abs (pH6.0/4.5)}}$ triggered by pH switch from 6.0 back to 4.5. In both cases the bending signal (the vertical difference between the blue squares in Figure S2) was calculated by subtracting the intersection value of the fitted curve obtained at pH 6.0 from the intersection value of the fitted curve obtained at pH 4.5. The resulting bending signals obtained from the IDL software were converted to measures of absolute stress using Stoney's equation (Equation 1), with $L = 450 \mu\text{m}$, giving $\Delta \sigma_{\text{abs}} = 0.24067 \Delta z_{\text{abs}}$. Please note that more significant figures have been used in the calculations than are shown in Tables S2 and S3 presented later in this section. This method of measuring the stresses has two consequences. Firstly the contrast between deprotonation and protonation will be confounded with any order effect, since deprotonation is always measured first. Secondly the within-cantilever measurement errors, e_{sti1} and e_{sti2} , defined below, could be correlated (allowance is made for this in the analysis).

The ANOVA was based upon a linear model, (Equation S1), which describes how the absolute stress, hereafter termed y , depends on the various fixed and random factors. A general introduction to the ANOVA is given in standard text books²⁰. Let y_{stik} be the k th observation on the i th cantilever in the (st) th cell (Array s and SAM t), then:

$$y_{stik} = M + A_s + T_t + (AT)_{st} + u_{sti} + P_k + (AP)_{sk} + (TP)_{tk} + (ATP)_{stk} + e_{stik} \quad (\text{Equation S1})$$

with $k = 1, 2; i = 1, \dots, n_{st}; t = 1, 2; s = 1, 2, 3, 4$; where appropriate constraints are put on the fixed parameters (to remove redundancy). The random errors, u_{sti} and e_{stik} , are assumed to be normally

distributed with variances σ_u^2 and σ_e^2 , respectively. The correlation between e_{sti1} and e_{sti2} is ρ , but otherwise all u 's and e 's are assumed to be independent. The within-cantilever random error, e_{stik} , models the unexplained or residual variation for a single cantilever, while the between-cantilever error, u_{sti} , accounts for the extra differences between cantilevers (in the same array and with the same SAM) over and above that which would arise from the within-cantilever variation. The parameters A_s , T_t , P_k represent the main effects of the three fixed factors, cantilever array, SAM, and deprotonation/protonation, respectively. The remaining parameters are the two and three term interactions of these three factors. The number, n_{st} , of cantilevers in each Array by SAM cell are given in Table S1. Ideally, and by our design, each cantilever array would contain the same number (four) of cantilevers coated with MHA as with HDT, however, as explained earlier some cantilevers could not be used.

Table S1: Number n_{st} of cantilevers in each array by SAM cell.

SAM (<i>t</i>)	Array (<i>s</i>)				Totals $\sum_s n_{st}$
	1	2	3	4	
1 (HDT)	3	2	2	2	9
2 (MHA)	3	2	2	3	10
Totals $\sum_t n_{st}$	6	4	4	5	19

Table S2 gives the absolute stresses for these 19 cantilevers, the means and the differences for the deprotonation and protonation pairs, and the Array by SAM cell means. On examination Array 3 appears atypical. For our purpose, which is to gain understanding of the processes, it is important to retain atypical results, although, before the technology is ready to be used diagnostically, some further inclusion/exclusion protocols may need to be developed.

Table S2: Table of data, means, and differences.

*SAM: $t = 1$ for HDT, $t = 2$ for MHA.

Array (s)	SAM* (t)	Cantilever $i(st)$	Deprotonation (y _{sti}) [mN/m]	Protonation (y _{stz}) [mN/m]	Mean [mN/m] $1/2(y_{sti} + y_{stz})$	Difference [mN/m] (y _{sti} - y _{stz})
1	1	1	-8.50	-8.40	-8.45	-0.10
1	1	2	-9.51	-9.24	-9.37	-0.26
1	1	3	-8.52	-8.23	-8.38	-0.29
1	1	Mean	-8.84	-8.62	-8.73	-0.22
1	2	1	-7.70	-7.51	-7.61	-0.19
1	2	2	-7.89	-7.58	-7.74	-0.31
1	2	3	-7.63	-7.48	-7.56	-0.14
1	2	Mean	-7.74	-7.52	-7.64	-0.21
2	1	1	-7.73	-7.32	-7.52	-0.41
2	1	2	-6.93	-6.74	-6.84	-0.19
2	1	Mean	-7.33	-7.03	-7.18	-0.30
2	2	1	-6.28	-5.68	-5.98	-0.60
2	2	2	-6.76	-6.45	-6.61	-0.31
2	2	Mean	-6.52	-6.06	-6.29	-0.46
3	1	1	-1.42	-1.83	-1.62	0.41
3	1	2	-0.96	-1.44	-1.20	0.48
3	1	Mean	-1.19	-1.64	-1.41	0.45
3	2	1	1.54	1.37	1.46	0.17
3	2	2	0.00	-0.34	-0.17	0.34
3	2	Mean	0.77	0.52	0.64	0.25
4	1	1	-5.17	-5.22	-5.20	0.05
4	1	2	-5.44	-5.49	-5.46	0.05
4	1	Mean	-5.31	-5.35	-5.33	0.05
4	2	1	-5.13	-4.86	-4.99	-0.26
4	2	2	-4.21	-3.87	-4.04	-0.34
4	2	3	-4.19	-4.00	-4.09	-0.19
4	2	Mean	-4.51	-4.24	-4.38	-0.26
Grand Mean						-5.34 mN/m

The ANOVA partitions the Corrected Total Sum of Squares $\sum_s \sum_t \sum_i \sum_k (y_{stik} - \bar{y}_{\dots})^2 = 335.26$

according to the individual Sources of Variability, where

$\bar{y}_{\dots} = (1/38) \sum_s \sum_t \sum_i \sum_k y_{stik} = -5.34 \text{ mN/m}$. The resultant ANOVA table is shown in Table S3.

Each of rows 2 to 10 in Table S3 corresponds to a factor, an interaction or a random term in the model (Equation S1).

Table S3: ANOVA for the cantilever array data.

	1	2	3	4	5	6	7
	Sources of Variability						
1	Sources of Variability	DF*	Sequential Sum of Squares [(mN/m) ²]	Adjusted Sum of Squares [(mN/m) ²]	Sequential Mean Square [(mN/m) ²]	F-value	p-value
2	Array	3	312.368	311.229	104.123	185.58	< 0.0005
3	SAM	1	14.003	14.263	14.003	24.96	< 0.0005
4	Array × SAM	3	1.841	1.841	0.614	1.09	0.392
5	Between-Cantilever Error	11	6.172	6.172	0.561	95.34	< 0.0005
6	Deprotonation/Protonation	1	0.118	0.072	0.118	20.06	0.001
7	Array × Deprotonation/Protonation	3	0.602	0.600	0.201	34.12	< 0.0005
8	SAM × Deprotonation/Protonation	1	0.056	0.063	0.056	9.49	0.010
9	Array × SAM × Deprotonation/Protonation	3	0.034	0.034	0.011	1.91	0.187
10	Within-Cantilever Error	11	0.065	0.065	0.006		
11	Corrected Total	37	335.259				

* **DF: Degrees of freedom.**

The Sequential Sum of Squares given in column 3 of Table S3 corresponds to the decrease in the residual sum of squares when a new term is added to the model containing all those terms added prior to this new term (terms were added in the order shown in the table). Conversely, the Adjusted Sum of Squares given in column 4 corresponds to the decrease in the residual sum of squares when a new term enters a model which already contains all the other terms. Here we use the sequential sum of squares as we are primarily interested in the effects which arose from the difference in the SAM cantilever coating. However, the use of the adjusted sum of squares was found not to alter the qualitative results of the ANOVA. The Sequential Mean Squares given in column 5 of Table S3 were obtained by dividing a sequential sum of squares by its Degrees of Freedom, given in column 2 of Table S3. The F -value given in column 6 of Table S3 is the mean square ratio, *i.e.*, the mean square for a particular source of variability divided by the mean square for its associated random error term. The p -value in column 7 of Table S3 is the probability of obtaining such a large F -value if the true value of the relevant parameters were zero. A small p -value is interpreted as evidence that the relevant parameters are not zero.

The Within-Cantilever Error mean square in row 10 estimates the *effective* within-cantilever error variance, $\sigma_e^2 (1 - \rho)$, and Between-Cantilever Error mean square in row 5 estimates the *total* between-cantilever error variance, $\sigma_e^2 (1 + \rho) + 2\sigma_u^2$. From the F - and p -values in row 5 there is clear evidence that the *total* between-cantilever error variance is greater than the *effective* within-cantilever error variance, however, we cannot determine how much this is due to σ_u^2 rather than to ρ . Fortunately, the interpretation of the rest of the ANOVA table is not affected. Deprotonation/Protonation and its interactions with Array and SAM in the lower half of Table S3 involve only within-cantilever variation as the deprotonation and protonation reactions were observed on the same cantilever, so the appropriate random variation term is the mean square 0.006 in row 10. This allows quite small main effects and interactions to be detected (rows 6, 7, and 8).

There is evidence that the magnitude of the absolute deprotonation stress tends to be slightly more negative (compressive) than the absolute protonation stress, and that the size of this difference varies between SAMs (greater for MHA than for HDT) and between cantilever arrays. Array, SAM, and Array by SAM in the upper half of Table S3, involve the total between-cantilever error variance, so the appropriate denominator mean square is 0.562 in row 5. From the F - and p -values in rows 2, 3, and 4, we conclude that there is clear evidence of differences between cantilever arrays and between SAMs but no evidence of an interaction. This is important as it suggests that the differential stress will not change from one cantilever array to another. To estimate the differential stress between MHA and HDT we used $(1/4) \sum_s (\bar{y}_{s2\cdot} - \bar{y}_{s1\cdot}) = 1.24$ mN/m. This has standard error $\sqrt{(7/64) (\sigma_e^2 (1 + \rho) + 2\sigma_u^2)}$, where $\bar{y}_{st\cdot} = (1/2n_{st}) \sum_i \sum_k y_{stik}$ is the (st) th cell mean. Using the mean square in row 5 to estimate $(\sigma_e^2 (1 + \rho) + 2\sigma_u^2)$ gives an estimated standard error of 0.24 mN/m. Finally, it is useful to estimate the change in differential stress between protonation and deprotonation. We averaged the estimates for each array, giving $(1/4) \sum_s ((\bar{y}_{s2\cdot 2} - \bar{y}_{s1\cdot 2}) - (\bar{y}_{s2\cdot 1} - \bar{y}_{s1\cdot 1})) = 0.18$ mN/m with standard error $\sqrt{(7/16) \sigma_e^2 (1 - \rho)}$. When the residual error mean square (row 10) is substituted for $\sigma_e^2 (1 - \rho)$, this gives an estimated standard error of 0.05 mN/m. Thus the study has shown that from the 38 observations for pH 6.0 and using sodium phosphate solutions we were able to estimate the differential stress with a relative standard error of about 20 per cent. Under these conditions the differential stress was tensile. The measurement of differential stress made during protonation was slightly more positive (tensile) than during deprotonation, the difference being measured in our experiment with a relative standard error of about 30 per cent.

Future experiments to investigate the kinetics of surface stress evolution will include investigation of the use of non-linear functions to fit the raw data and further study of the nature and chemical

implications of different sources of variation, including the within- and between-cantilever effects of successive cycles and measurement order²¹.